Advances in Manufacturing of Molded Tips for Scanning Probe Microscopy

Nicolaie Moldovan, Zhenting Dai, Hongjun Zeng, *Senior Member, IEEE*, John A. Carlisle, Tevis D. B. Jacobs, Vahid Vahdat, David S. Grierson, Jingjing Liu, Kevin T. Turner, and Robert W. Carpick

***Abstract*—A common method for producing sharp tips used in scanning probe microscopy (SPM) and other applications involving nanoscale tips is to deposit thin-film materials, such as metals, silicon nitride, or diamond-based films, into four-faceted pyramidal molds that are formed by anisotropic etching into a (100) silicon substrate. This well-established method is capable of producing tips with radii as small as a few nanometers. However, the shape of the tip apex is difficult to control with this method, and wedge-shaped tips that are elongated in one dimension are often obtained. This limitation arises due to the practical difficulty of having four planes intersecting at a single point. Here, a new method for producing three-sided molds for SPM tips is demonstrated through the use of etching in (311) silicon wafers. It is shown that silicon nitride and ultrananocrystalline diamond tips fabricated with this new method are wedge free and sharp ($<$ 10 nm radius), thereby restoring tip molding as a well-controlled manufacturing process for producing ultrasharp SPM tips. [2011-0209]**

***Index Terms*—Atomic force microscopy (AFM), crystallographic etching, molding, scanning probe microscopy (SPM), silicon, tips.**

I. Introduction

TIP MOLDING is a well-known nanofabrication method for producing ultrasharp tips, such as those used in scanning probe microscopy (SPM) [1]–[3], field emitters [4], [5], vacuum electronics [6], [7], or tunneling-based devices [8]. Tip molding consists of etching a pyramid-shaped pit into a sacrificial substrate (typically silicon), depositing the desired thin-film material into the mold, processing further to define other features in the deposited material such as a cantilever arm, and then removing the sacrificial substrate to reveal a pyramid-shaped tip. The most common mold geometry is a square (four-sided) pyramid etched into a Si (100) wafer via anisotropic etching [9], [10] in an alkaline solution (e.g., potassium hydroxide (KOH), tetramethylammonium hydroxide, Ethylenediamine and pyrocathechol, or others). Such molds are four-faceted pyramids, with each facet belonging to the slow-etching $\{111\}$ family of planes. Indeed, we have shown that monolithic ultrananocrystalline diamond (UNCD) atomic force microscopy (AFM) probes with integrated tips can be formed with this method, and the tips show exceptional wear resistance under harsh conditions compared to molded silicon nitride tips [11].

Additionally, such pits can be sharpened by oxidation [12], which improves the aspect ratio and lowers the radius at the bottom of the pit. Square pyramids in Si (100) wafers can be produced by patterning either perfect squares or circles into a hard mask layer, such as SiO_2, Si_3N_4, or certain metals, used to protect the surrounding Si. While tip radii in the few-nanometer range can be obtained [13] [shown in Fig. 1(a)], it is common to produce tips that are elongated in one dimension and reach a form of a wedge [shown in Fig. 1(b)]. This wedge shape originates from the four facets of the pyramidal mold not meeting at a single point, whereas the size of the wedge depends on the precision of the lithography and etching. Optical lithography can control the equality of adjacent sides of squares or circle eccentricities only down to 20–50 nm, due to factors such as illumination nonuniformities, mask imperfections, proximity effects in the aerial image, and concentration gradients in the developer. The sidewall roughness of the resist ($\sim$10 nm) falls in the same range, while transfer of the resist pattern into the hard mask pattern copies or even amplifies this roughness. Some additional variability in the feature size also comes from the misorientation of the Si wafer plane from the ideal crystallographic (100) plane (typically $\sim 0.5^\circ$) and from proximity effects in etching (both of the hard mask and the Si) related to plasma or solution concentration gradients (such as produced by stirring and bubbling). Thus, the wedge size on four-faceted pyramidal molds can be controlled only to the limit of tens of nanometers.

Fig. 2 shows typical distributions (squares) of wedge sizes obtained from an optimized fabrication process for making pyramidal tip molds and shows median wedge sizes of tens of nanometers in two representative runs. If oxidation

Manuscript received July 18, 2011; revised September 7, 2011; accepted September 30, 2011. Date of publication December 2, 2011; date of current version April 4, 2012. This work was supported in part by the National Science Foundation (NSF) through the Small Business Technology Transfer Program under Phase II and Phase IIB Grants 0638030 and 0823002 and in part by the Nano/Bio Interface Center under NSF Nanoscale Science and Engineering Center Award DMR08-32802. The work of K. T. Turner was supported by the NSF Civil, Mechanical and Manufacturing Innovation (CMMI) Division under Grant 0825000. The work of R. W. Carpick was supported by the NSF CMMI Division under Grant 0826076. Subject Editor R. R. A. Syms.

N. Moldovan, Z. Dai, H. Zeng, and J. A. Carlisle are with Advanced Diamond Technologies, Inc., Romeoville, IL 60446 USA (e-mail: moldovan@thindiamond.com; zdai@thindiamond.com; zeng@thindiamond.com; carlisle@thindiamond.com).

T. D. B. Jacobs, V. Vahdat, and R. W. Carpick are with the University of Pennsylvania, Philadelphia, PA 19104 USA (e-mail: carpick@seas.upenn.edu).

D. S. Grierson was with the University of Wisconsin, Madison, WI 53706 USA. He is now with systeMECH, LLC, Madison, WI 53703 USA.

J. Liu was with the University of Wisconsin, Madison, WI 53706 USA. She is now with Applied Materials, Inc., Santa Clara, CA 95054-3299 USA.

K. T. Turner was with the University of Wisconsin, Madison, WI 53706 USA. He is now with the University of Pennsylvania, Philadelphia, PA 19104 USA (e-mail: kturner@seas.upenn.edu).

Color versions of one or more of the figures in this paper are available online at http://ieeexplore.ieee.org.

Digital Object Identifier 10.1109/JMEMS.2011.2174430

1057-7157/$26.00 © 2011 IEEE

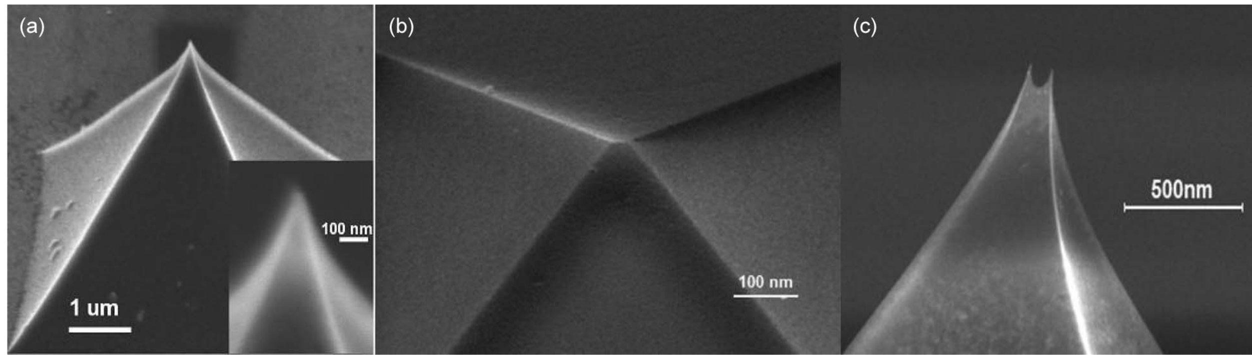

Fig. 1. SEM images of tips formed from different four-faceted Si (100) molds. (a) "Perfect" UNCD tip molded into an oxidation-sharpened wedge-free V-groove in a Si (100) mold. (Inset) High-resolution image of the tip. (b) UNCD tip molded into a wedge-ended Si (100) imperfect and unsharpened V-groove. (c) UNCD tip molded into an oxidation-sharpened V-groove in Si (100), which is similar to the one in (b) before oxidation. Statistics show that, after oxidation sharpening, double tips separated by less than 25 nm cannot be seen, indicating that smaller wedges collapse into a single tip. Oxidation-sharpened tips, including each of the double tips, have radii consistently < 10 nm.

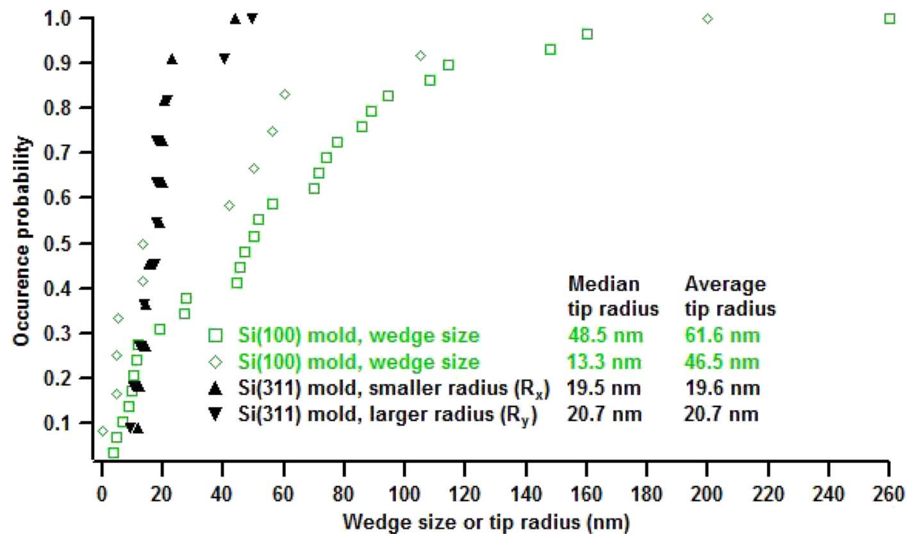

Fig. 2. (Green square markers) Wedge size distributions in four-faceted pyramids obtained on Si (100) by KOH etching starting from an oxide hard mask structured into circles with optical lithography—two runs from previous study [25]. (Black triangle markers) Principal tip radii of diamond probes obtained on Si (311)—this study.

sharpening is used, wedges smaller than ~25 nm will collapse to single-point tips. However, larger wedges generate double tips, as shown in Fig. 1(c), rendering them unusable for most applications including AFM-based imaging. While the average size of a wedge-shaped tip is relatively small, the variance can be significant, requiring additional quality control (QC) steps to discriminate and exclude the oversized wedge tips. Precise QC requires piece-by-piece inspection using scanning electron microscopy (SEM), transmission electron microscopy (TEM), or AFM, which can be tedious and time consuming. Not only is such inspection impractical and cost prohibitive for high-throughput manufacturing, but it can also result in contamination or damage of the tips during examination.

Because of these challenges, many manufacturers have migrated away from molding technology for SPM tip fabrication. For instance, traditional SPM probes made of monolithic Si_3N_4 have been gradually replaced by Si_3N_4-coated Si tips. However, coated tips have their own limitations. While Si tips can be fabricated consistently with tip radii in the sub-10-nm range [14], [15], adding the Si_3N_4 layer increases the tip radius in proportion to the thickness of the coating (10- to 20-nm range). Similar problems have been observed with metal- [16], SiC-, and diamond-coated probes [17], [18]. In some cases, the minimum film thickness is limited by the deposition process or by the electrical resistance requirements for the coated films, which can substantially increase the tip radius. This is the situation for diamond-coated silicon tips, where tip radii are usually in the 50-nm range or larger.

Various improvements to the tip-molding approach have been proposed [19]–[22]. In one method [20], etch shapes can be designed to intentionally create large wedges at the end of etched pits, which, followed by oxidation sharpening, produce two separated sharpened tips, one at either end of the wedge. However, it is difficult to reliably place the two tips to ensure that they do not interfere with each other in the scanning process. This limits the useful height of such probes in the direction along the cantilever, losing the advantage of the overall height of the pyramid, which becomes irrelevant. While longer wedges can be designed to separate the two tips better, elongated pyramidal molds have negative consequences

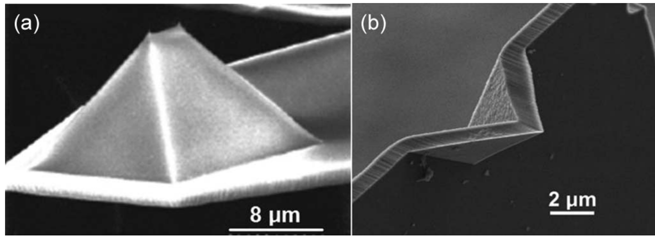

Fig. 3. Methods to avoid wedged tips in molding technology. (a) "Twin-tip"-elongated wedge probe from Olympus (OMCL-HA100WS, [20]—publication permit granted). (b) Two-side-molded one-side-etched ("Tomie") UNCD probe (experimental work performed by the present authors).

on probe reflectivity, stiffness, and resonance frequency [Fig. 3(a)]. Another method, possibly augmenting the molding method, involves using reactive-ion etching (RIE) of the tip material after the mold has been filled to remove all material ahead of the wedge-shaped pit [Fig. 3(b)]. This is equivalent to cutting off the wedge-problem area and limiting the tip by three planes, two obtained by molding and one obtained by etching. While such tips have the advantage of being placed at the very end of the supporting cantilevers, the sharpness of the tips is mostly limited by the imprecision of the RIE cut into the deep tilted wedges. For such probes, the radii are typically $\sim$35 nm, and furthermore, the aspect ratio is too low for many applications [19].

In the present work, a new fabrication method is demonstrated to produce ultrasharp tips via molding using three-sided pyramidal molds etched into (311)-oriented Si wafers. The method is compatible with oxidation sharpening to generate high-aspect-ratio tips. The method was successfully tested using Si_3N_4 and conductive UNCD [23] as structural tip materials, showing the complete elimination of wedges and a robust tolerance to lithographic imperfections and alignment imprecision with respect to the crystallographic orientation. Tip radii were consistently measured to be below 10 nm with oxidation sharpening and below 20 nm without oxidation sharpening (the triangles in Fig. 2), with significant narrowing of the distribution curve in the large tip radius range.

II. Crystallographic Considerations

The idea of using a custom-oriented Si wafer for wedge-free tip fabrication can be better understood by considering oxidation-sharpened alignment marks used for molding-based fabrication of UNCD probes on Si (100) wafers [24]. Such alignment marks consist of four elongated wedged V-grooves, arranged to form an alignment cross. Fig. 4 shows a UNCD structure molded and released from such a wedge structure, showing particularly sharp spikes at both ends of the wedge. Those spikes are always produced by oxidation sharpening at the intersection of three Si $\{111\}$ facets. The spike axis orientation is differently tilted with respect to the three edges of the trihedron. Its orientation is approximately pointing in the $\langle 100\rangle$ direction, as do the spikes from perfect four-faceted pyramids. Choosing a crystallographic wafer plane tilted with respect to the Si (100) plane in a convenient way [e.g., such as that shown in Fig. 4(b) and (c)] may result in trihedral molds and tips.

A more detailed analysis in Fig. 5 shows a portion of the Si crystal lattice with symmetrical face-centered cubic (fcc) unit cells such as $ABCDA'B'C'D'$ and other vicinal cells. A wedge V-groove, like the ones shown in Fig. 4, can be represented by the geometrical figure $MNR'T'VV'$.

The facets $VMT'V'$, $VNR'V'$, and VMN belong to the Si $\{111\}$ family. If we consider a point L on the direction VV' and the plane determined by the points L, M, and N, we get the family of planes which one can choose as wafer orientations such that the V-grooves formed by alkaline etching result in a triangular-base pyramid (i.e., the family of pyramids $VLMN$, with $L \in VV'$). There are several ways to choose these planes, such that convenient symmetries characterize the $VLMN$ pyramids. One convenient way is to choose the plane such that the edges of the pyramid are equal to each other $(VM = VN = VL = MN)$. In this case, the point L coincides with D', and one can show that the plane $D'MN$ is the (1, $\bar{1}$, 3) plane, a member of the $\{311\}$ family. In this approach, one can demonstrate that the edges of the pyramid are equally tilted with respect to the wafer plane, which is another interesting symmetry feature. Another high-symmetry choice of the wafer plane would be such that the tilt of the plane VMN with respect to the plane LNM is equal to the tilt of the edge VL with respect to the plane LMN. In this case, both longitudinal and transversal cross sections of the tip would be isosceles triangles. In this case, the wafer plane (LMN) would have irrational Miller indices (close to $\{11, 10, 29\}$), and the point L lays between V and D'; the angle between this plane and the (311) plane would be $\sim 7.22°$. In general, planes with Miller indices belonging to the family $\{khh\}$, with $1 < k/h \leq 3$, or close to them will generate triangular-base pyramids. While all these choices are available for custom-oriented wafers, practicality requires the selection of planes with the lowest possible Miller indices. Aside from the dominant orientations Si (100), Si (111), and Si (110), silicon wafers with (311) and (522) orientations are available, with Si (522) being less common than Si (311). Thus, Si (311) is the best choice. In the case of Si (311), the mold pyramids and resultant tips will look like those in Fig. 6. The lateral facets of the pyramid are all $\{111\}$ facets, while the vertex V is at the intersection of three slow-etching planes, being as close to a single geometric point as the etching perfection can provide.

III. Experiments With Si (311) Wafers for Tip Fabrication

Several process experiments were performed on Si (311) wafers in order to demonstrate the three-faceted triangular-base pyramid formation, to investigate their shape variability as a function of lithography performance and mask design, and to study tip enhancement with oxidation sharpening. In addition, the molds were filled with both UNCD and low-stress silicon nitride, and the resulting tips were characterized.

In order to investigate the formation of three-faceted pyramids, a special test mask was designed which contained triangles of different sizes and orientations, as well as other test structures that are described later. The main triangles on the mask have the shape of isosceles triangles, MND' in Fig. 6,

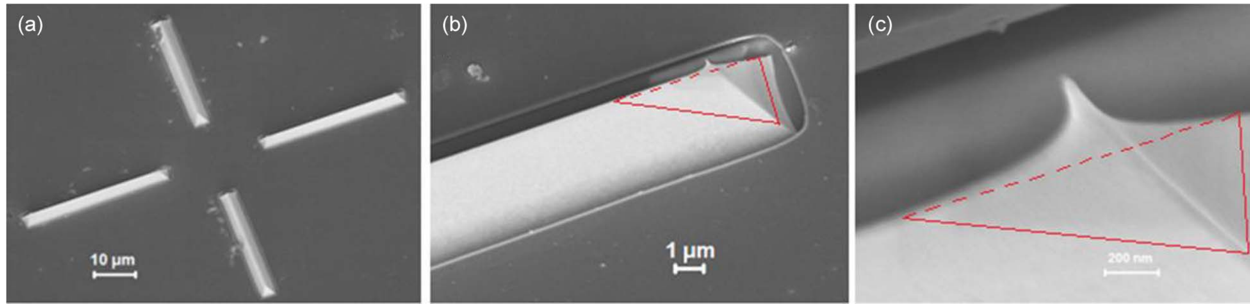

Fig. 4. (a) UNCD molded into a wedge-shaped oxidation-sharpened alignment mark used on Si (100) wafers for probe fabrication, showing sharp spikes at the intersection of three Si $\{111\}$ facets; (b) and (c) show successive levels of detail, with a sectioning plane marked as a possible wafer plane orientation that would result in triangle-base pyramids as V-grooves.

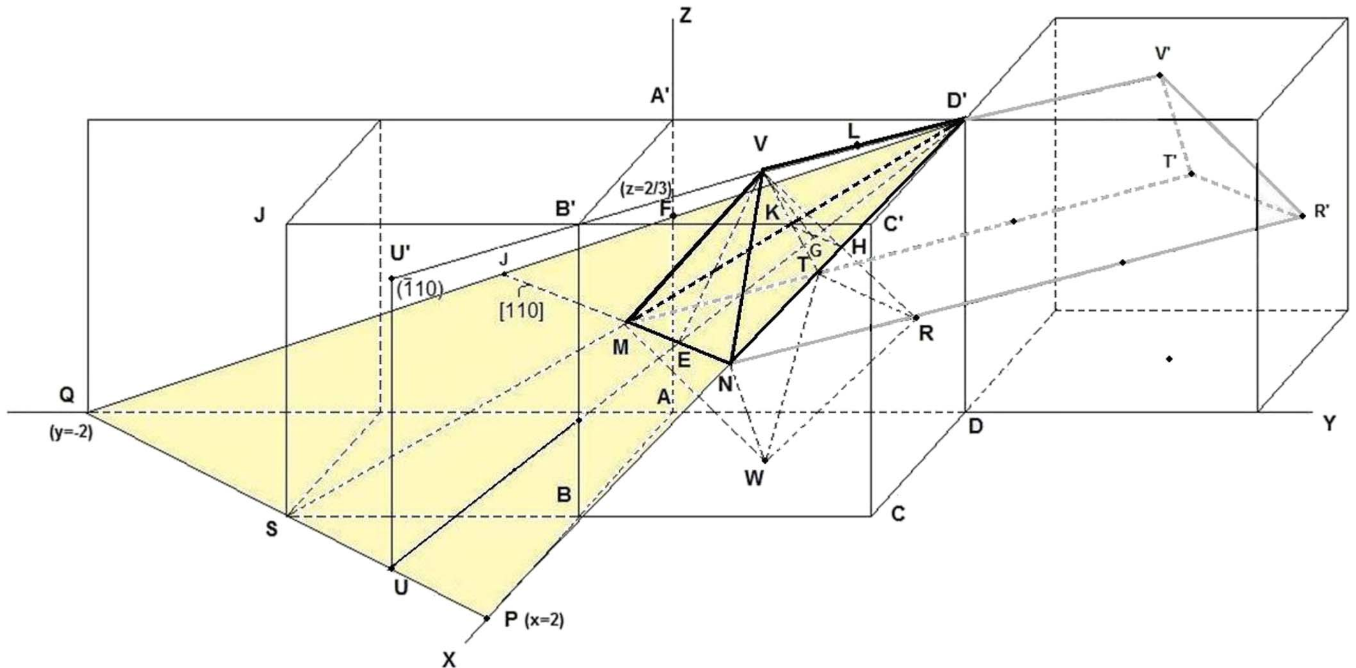

Fig. 5. Geometrical considerations for choosing a wafer plane to generate triangular-base pyramids as V-grooves. The cube $ABCDD'A'B'C'$ is the symmetrical unit cell (fcc) of Si, while the possible wafer planes discussed are the family of planes LMN, with $L \in VV'$. The tinted plane $D'QP$ corresponds to the crystallographic plane (1, $\overline{1}$, 3).

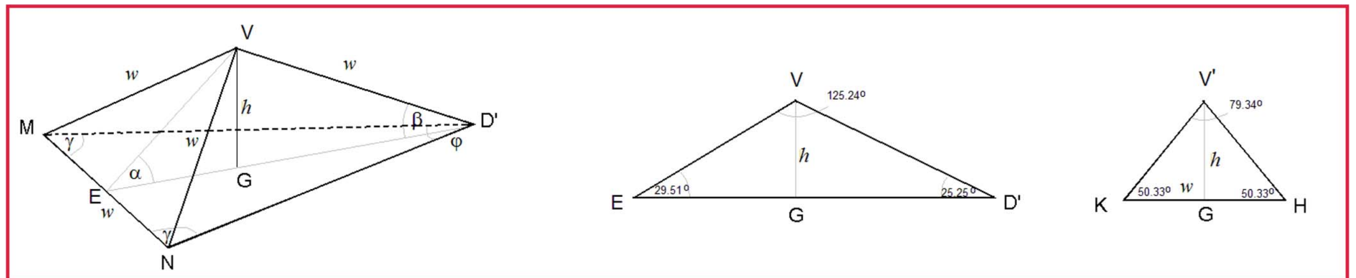

Fig. 6. Geometry of triangular-base pyramid pits that can be fabricated in Si (311) through anisotropic etching. The facets VMN, VND', and VMD' are all $\{111\}$ facets.

with the base angles $\gamma \approx 73.22^\circ$ $(\tan(\gamma) = \sqrt{11})$ and the top angle $(\varphi \approx 33.55^\circ)$ calculated from crystallographic considerations. In order to form the desired pyramids, these triangles have to be oriented properly with regard to the crystallographic axes. To achieve this, the wafers were single-side polished with a primary flat on the [110] direction and a second minor flat perpendicular to the primary one. Since the flats are processed on the ingot, all wafers/wafer flats were similarly oriented, avoiding ambiguities when flipping over the wafers. To determine the proper orientation of the masking triangle, the mask included control triangles with four positions, rotated by 90° from each other. Four Si (311) wafers were oxidized to a thickness of

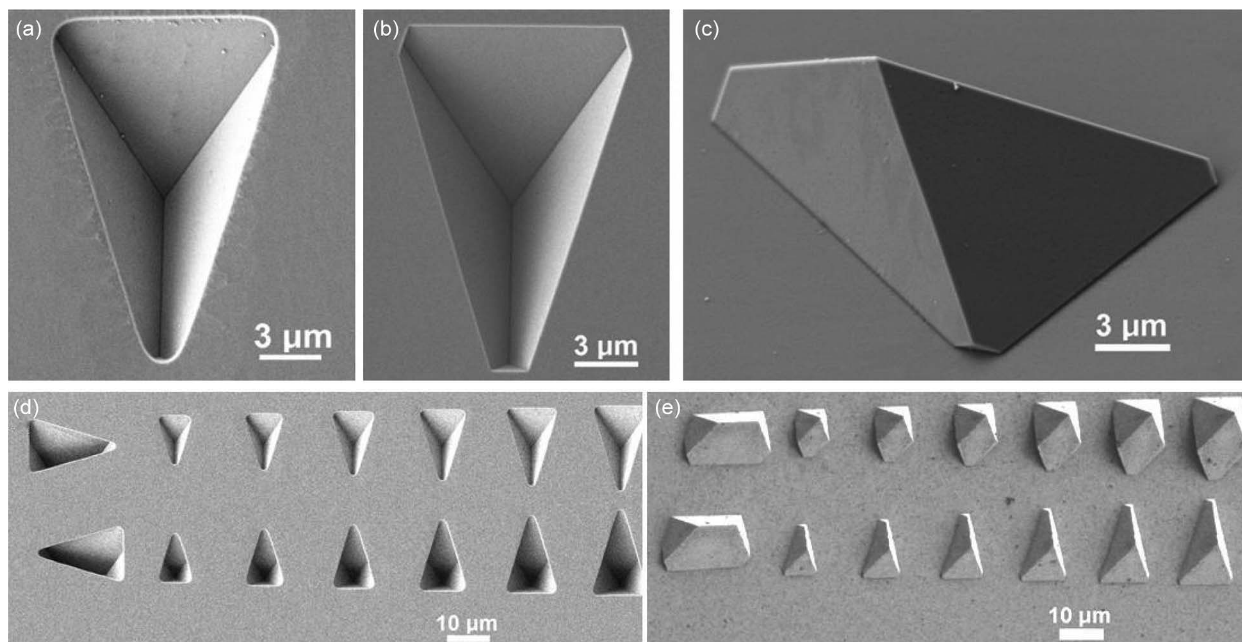

Fig. 7. Triangular-base pits etched in Si (311) and resulting molded tips. (a) Single etched pit, prior to the removal of the oxide mask, showing a clear formation of the three-faceted pyramid. (b) Single pit after the oxide hard mask was removed. Small facets form at the corners due to the rounding of the oxide. (c) UNCD tip molded in an etched pit, showing the formation of facets. (d) Test area with size variation and 90° rotation of some of the patterns. The upper row of triangles pointing down shows the correct orientation for generating trihedral tips. The larger triangles on the corners of the picture have equal base sizes of 11.72 μm, while the other triangles are scaled down with ratios of 11/12, 10/12, 9/12, 8/12, and 7/12, respectively. (e) Array of UNCD tips obtained from the test area shown in (d). The lower row of triangular-base pyramids is from molding in the upper triangular pits shown in (d).

350 nm; lithography and buffered oxide etching (BOE) were performed to pattern the oxide. The Si was subsequently etched in 30% KOH at 80 °C for 10 min to form the pits. Images of the pits were taken via SEM. Fig. 7(a) shows a top view of a pit prior to removing the masking oxide; the correct formation of the three-faceted pyramid can be recognized as agreeing with the geometry in Fig. 6. Imperfections in the lithography resulted in a slight rounding of the corners, where small Si {111} facets were generated. This can be better seen after the removal of the oxide [Fig. 7(b)] and in the images of a UNCD mold made in such a pit [Fig. 7(c)]. Fig. 7(d) presents a view of a test area with sequential rotations of 90°, showing that only the triangles with the sharp corner pointing in the [110] direction generate the desired pyramids. Fig. 7(e) shows a UNCD mold of such a test pattern.

A portion of the test mask was designed to study the sensitivity of the molded tip shape to the masking triangle's opening angle (Fig. 8). Triangles with top opening angle less than the nominal value (33.55°) generated small facets at the base corners [Fig. 8(b)], while triangles with larger opening angles generated a facet at the top corner [Fig. 8(c)]. However, the central tip region at the bottom of the mold was consistent for all triangle shapes, all possessing sharp tips and high aspect ratios.

Another portion of the test mask provided insight into the sensitivity of pit geometry with the relative tilt angle between the mask triangle and crystallographic orientation (Fig. 9). It is obvious that the triangle tilt results in the formation of small spurious facets at the base of the triangles, but the tip region remains well defined at the intersection of three Si (111) facets. The opening angle variation and the tilt variation studies prove that the Si (311) solution for wedge-shape elimination is extremely robust and stable with the primary variations in the lithographic process.

Two of the wafers with triangular-base pyramidal pits were oxidation sharpened using a recipe that produces a 500-nm oxide on Si (100) facets. To investigate the pit shapes, molded tips were created by depositing 500 nm of low-stress nitride (LSN) using low-pressure chemical vapor deposition (LPCVD) on two wafers (one sharpened and one not sharpened) and by depositing 1 μm of UNCD on the other two (one sharpened and one not sharpened). The LPCVD LSN film was used in the experiment due to the high level of coating conformity to reveal the details of the Si (311) molds; however, charging effects due to the insulating nature of the nitride were expected to hinder the high-resolution SEM imaging. In contrast, the UNCD films were boron doped to low resistivity (0.05–0.08 $\Omega \cdot$ cm) to prevent charging effects, but the tip-filling conformity was expected to be slightly worse than the LPCVD nitride. Membranes made of both films were released from the back side of the wafers by KOH etching, and subsequent buffered HF etching (BOE 10%) removed the oxide from the oxidized wafers. Pieces of these membranes were detached and imaged with SEM and TEM.

Typical geometries for the unsharpened pyramids of molded UNCD are shown in Fig. 7(c) and (e). Fig. 10 shows the result of molding LSN into an oxidation-sharpened pyramid pit. One can see the formation of oxidation-sharpened spikes at all the trihedral joints between three Si (111) facets, including at the spurious facets appearing at the bottom corners of the pyramid. This can be better seen on a smaller-scale structure, which allowed a simultaneous view of both spikes at the upper right edge of the main pyramid [Fig. 10(c)]. The secondary

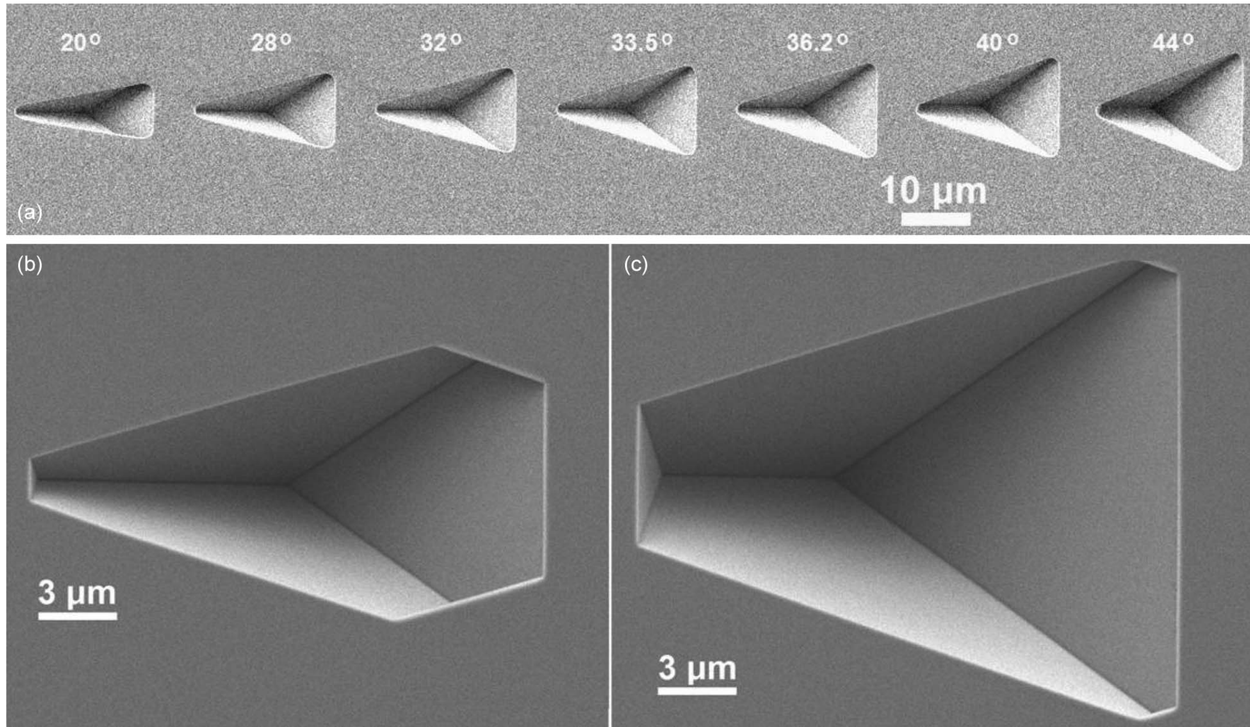

Fig. 8. Study of etched pit shape variation with the included angle of the triangle. (a) General view of the test area (covered with oxide). (b) Detailed view of the pit with the smallest angle (20°), showing spurious facets at the base corners (oxide removed). (c) Detail of the pit with the highest angle (44°), showing one larger facet at the left edge and small facets at the triangle base (oxide removed).

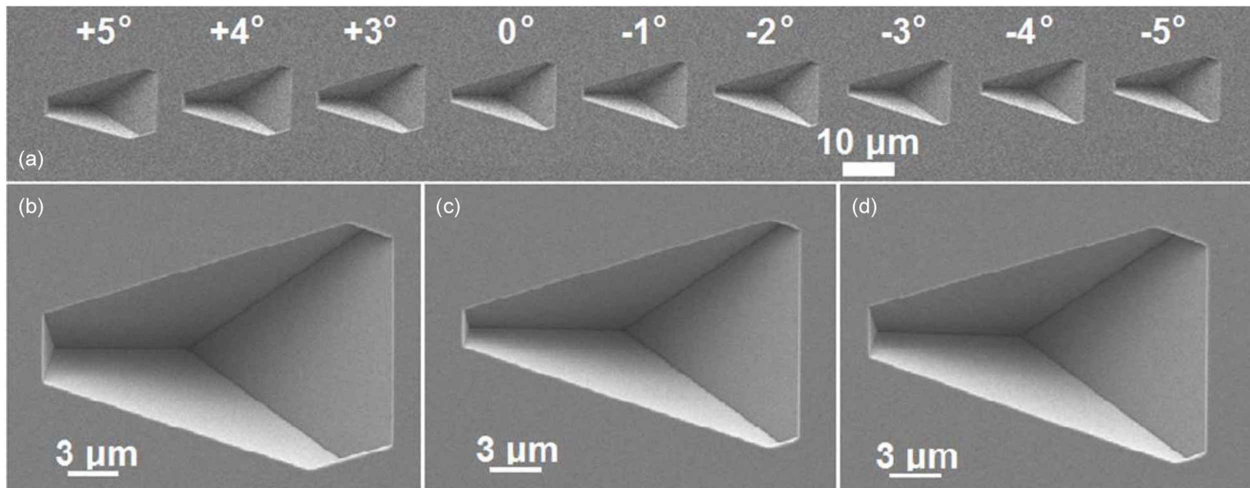

Fig. 9. Variation of pit formation with the misalignment of the triangle axis with respect to crystallographic orientation. (a) Resulting molds for sequential variation of the tilt angle, from $-5°$ to $+5°$. (b) Triangle with minimum tilt $(-5°)$. (c) Triangle with 0° tilt. (d) Triangle with maximum tilt $(+5°)$.

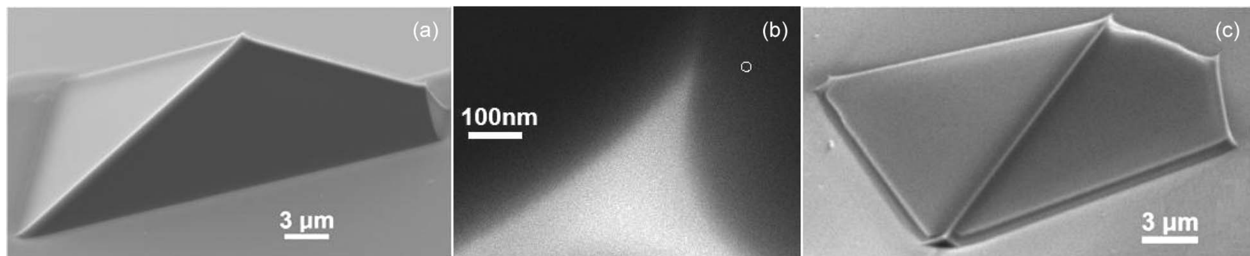

Fig. 10. Low-stress silicon nitride tips that were molded into oxidation-sharpened pyramids. (a) General view of a pyramid. (b) Higher-magnification image of the central spike with an estimated radius of < 10 nm (limited by SEM imaging resolution). The circle inset at the right of the tip has a radius of 10 nm. (c) Smaller-scale pyramid showing the formation of spikes at all spurious three-faceted corners.

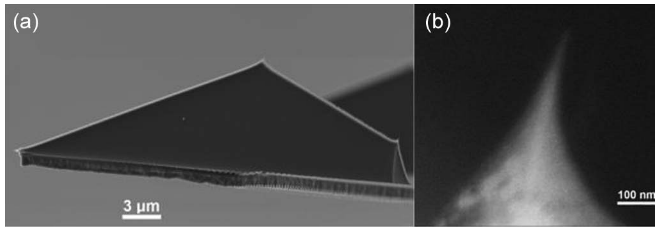

Fig. 11. UNCD molded into oxidation-sharpened pyramids. (a) General low-magnification view. (b) High-magnification image of the apex of the tip showing filling of the tip with a translucent amorphous carbon material. The tip radius is measured to be less than 7 nm. The brighter opaque structures are diamond grain clusters.

spikes below the principal spike will not affect the imaging performance of AFM probes made by this approach due to their distance from the principal spike (approximately 4–5 μm, the height of the tips). Higher magnification SEM imaging to determine the tip radii was limited on the LSN tips by charging effects; however, we can state that tip radii were well below 20 nm and were consistent with those of images of other tips measured to be < 10 nm [Fig. 10(b)]. On structures obtained by molding conductive UNCD into sharpened pyramids, the general shapes looked similar to those observed with the LSN, and tips as sharp as < 7 nm were measured (Fig. 11). As a general comment, filling the pits with UNCD becomes easier as the solid angle of the pit increases; therefore, Si (311) molds are easier to fill than similar Si (100) molds.

One additional advantage of using Si (311) wafers for molds comes from the fact that $\{311\}$ facets etch much faster than (100) planes in alkaline solutions [24], such as with 30% KOH at 85 °C, used in this study. This reduces the wafer etching from about 350 to about 215 min. A more complete study of bulk micromachining with Si (311) wafers, including etching rates, anisotropy diagrams with various solutions, and ways to fabricate alignment marks on such wafers, will be presented elsewhere.

IV. Fabrication and Testing AFM Probes With Tips Molded in Si (311) Pits

Once the tip fabrication process was characterized, UNCD probes for AFM were fabricated using the Si (311) technique. While several different types of probes are currently under evaluation, the present work demonstrates the creation of dynamic-mode UNCD probes, molded in non-oxidation-sharpened pits. The nominal pit depth/tip height was chosen as 7.1 μm, corresponding to a mask-level isosceles-triangle base of 11.7 μm, the same as the structures shown in Fig. 7(a)–(c). The fabrication sequence is similar to the process described previously for UNCD tips molded in four-sided pyramids [11]. It comprised fabrication of the pyramidal molds, deposition of UNCD (3 μm thick), patterning the UNCD in the shape of cantilevers and chip bodies by RIE [25] through a plasma enhanced chemical vapor deposition (PECVD) SiO_2 mask, chemical mechanical planarization of the PECVD SiO_2 mask, anodic bonding to a prediced Pyrex 7740 wafer, dicing through the Pyrex 7740 wafer to complete the handling chip body formation, dissolution of the Si wafer from the back side (except a handling frame), and deposition of reflective Al coating (70 nm) on the back side of the cantilevers. Fig. 12(a) and (b) shows the SEM images of a 120-μm-long 32-μm-wide UNCD cantilever with the characteristic tip shape. Fig. 12(c) shows a SEM image with an approximate measurement of the tip radius in the lateral direction (perpendicular to the cantilever direction), resulting in a tip radius of $\sim$6 nm, while Fig. 12(d) shows a measurement in the longitudinal direction (along the cantilever), resulting in a tip radius of $\sim$19 nm. Statistics on tip radii performed on 12 tips showed that these results are consistent for unsharpened Si (311) molds, in that, when the mold was well filled, a minimum principal tip radius of less than 10 nm (typically < 7 nm) occurs in the lateral direction, while the maximum principal tip radius of less than 35 nm (typically < 20 nm) occurs in the longitudinal direction.

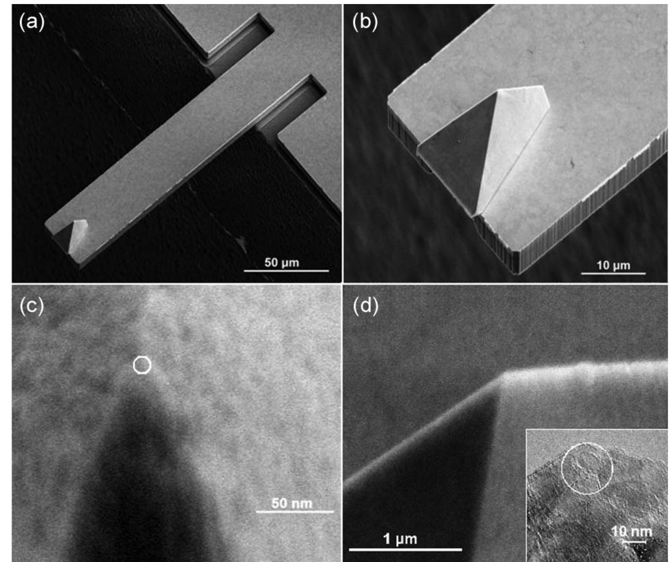

Fig. 12. Dynamic-mode AFM probes made of UNCD by molding in Si (311) pits. (a) General view of a cantilever. (b) Characteristic three-faceted pyramid integrated at the cantilever end. (c) Tip radius evaluation in the lateral direction with the circle showing a tip radius of $\sim$6 nm. (d) Tip radius evaluation in the longitudinal direction, with the inset showing a circle of radius 10 nm.

These results were confirmed by AFM imaging of test samples (NioProbe [26], TipCheck [27], and UNCD Aqua 25 [28] surfaces). The tool for probe evaluation was a Veeco NanoScope IIIa. Example images are shown in Figs. 13–15.

The NioProbe sample (Fig. 13) consists of a surface densely populated with random spikes of height $\sim$5 nm and is suited for investigating the immediate end of the AFM tip via either blind reconstruction algorithms or inverse tip imaging. The sample can be used for measuring the resolving capability of a tip down to $\sim$10 nm. Imaging of the NioProbe sample was performed with the UNCD probe in tapping mode with 366.2-kHz cantilever-driving frequency, 1-Hz scanning rate, and 25-nm tip vibration amplitude, as produced by a 67.2-mV driving amplitude of the actuating piezo crystal. The image reveals features of $\sim$10 nm in lateral size, demonstrating that the tip radius at the immediate apex is at or below the 10-nm level.

The TipCheck sample exhibits spike and edge features that are taller (in the range 100–140 nm) compared to those of

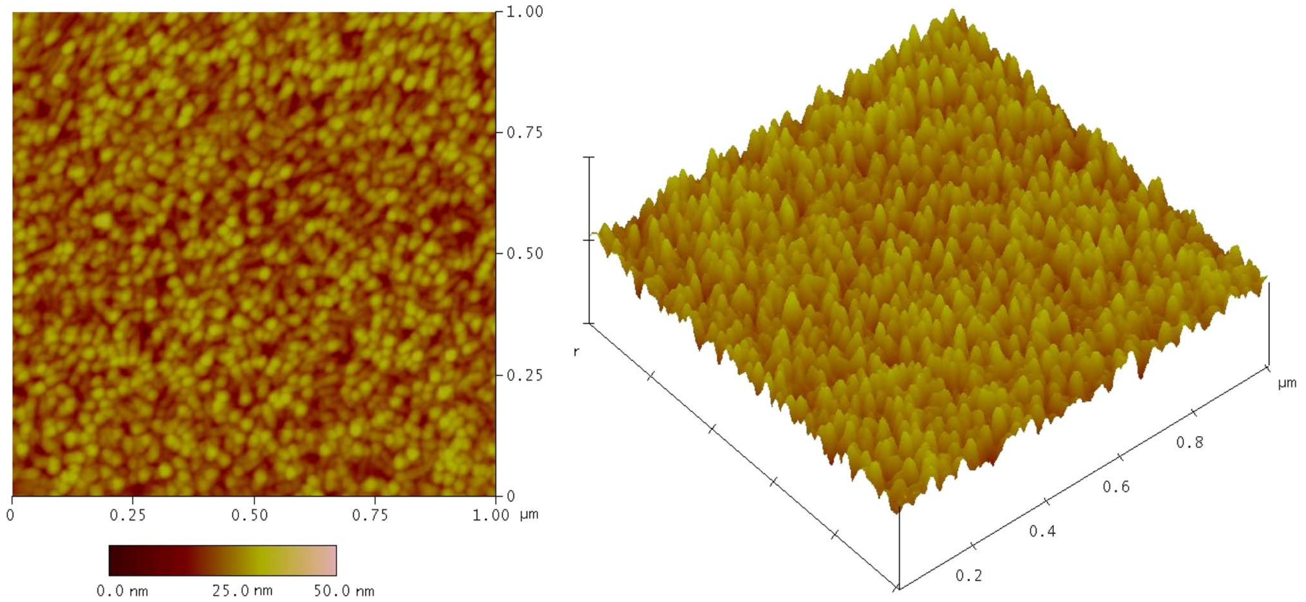

Fig. 13. Dynamic-mode images of a NioProbe test sample acquired with a three-faceted pyramid probe. The lateral resolution of the image is ∼10 nm, as determined by the size of the smallest features resolved.

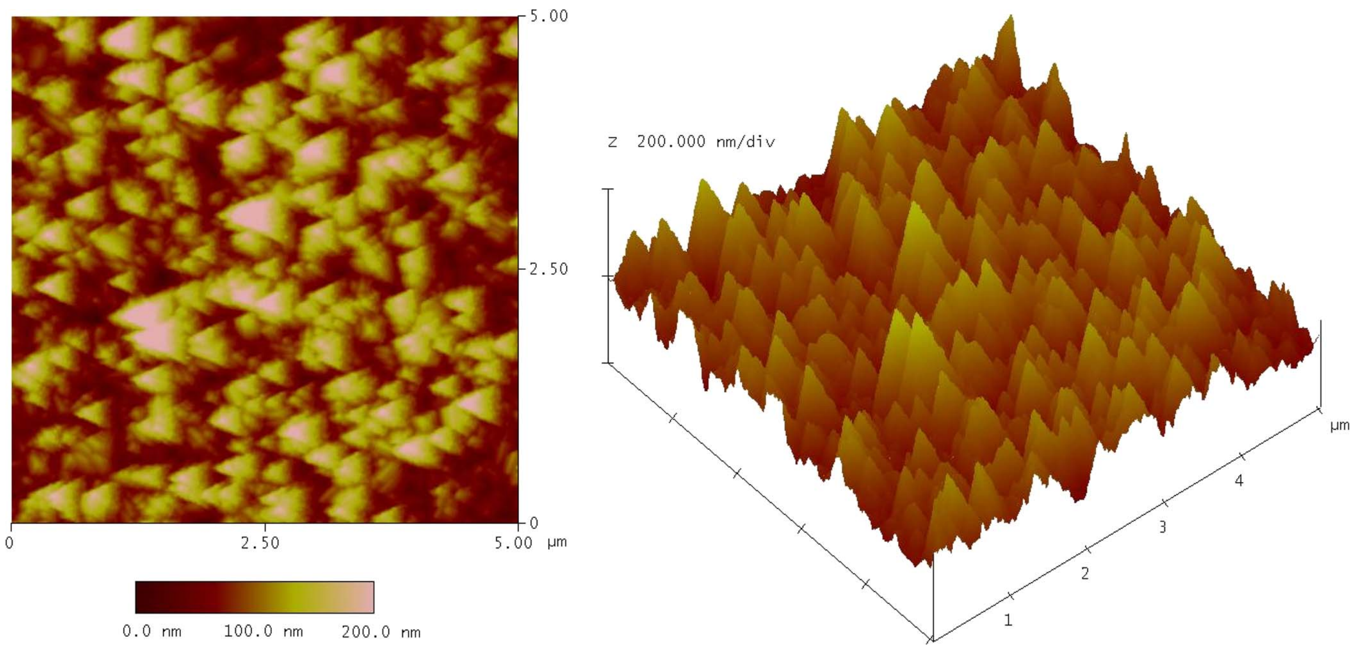

Fig. 14. Dynamic-mode imaging of a TipCheck test sample with the same three-faceted pyramid probe as that in Fig. 13.

the NioProbe sample and is used to characterize the tip shape beyond its immediate apex. The observation of repeated triangular features (the left image in Fig. 14) confirms that the pyramid shape is preserved below 100–140 nm from the tip apex. The 3-D image (the right image in Fig. 14) reveals repeated inverse images of the tip, with the sharpness of the spiked features demonstrating the sharpness of the tip apex.

The UNCD (Aqua 25) [28] test surface consists of faceted nanocrystalline grains in the 3- to 5-nm size range that form grain clusters, with a surface roughness of 10–20 nm (rms). The features on the UNCD surface are not as sharp as those on the NioProbe or TipCheck substrates but are more evenly distributed and with a rounded nanoscale texture. Therefore, a UNCD sample is able to provide consistent tip-shape characterization through blind reconstruction algorithms. The hardness and low-wear properties of diamond also minimize contamination and change of the substrate during scanning, and its high elastic modulus and low surface energy minimize elastic deformation induced by load and adhesion. All of these aspects suggest that UNCD samples are well suited for characterizing AFM tips made of hard materials. Fig. 15 shows the topographic image of such a surface with the tetrahedral UNCD probe. Blind tip reconstruction obtained by applying Scanning Probe Image Processor (SPIP) software [29] to images of the UNCD sample confirms quantitatively the values of the two principal tip-curvature radii as described before. Fig. 16 shows the

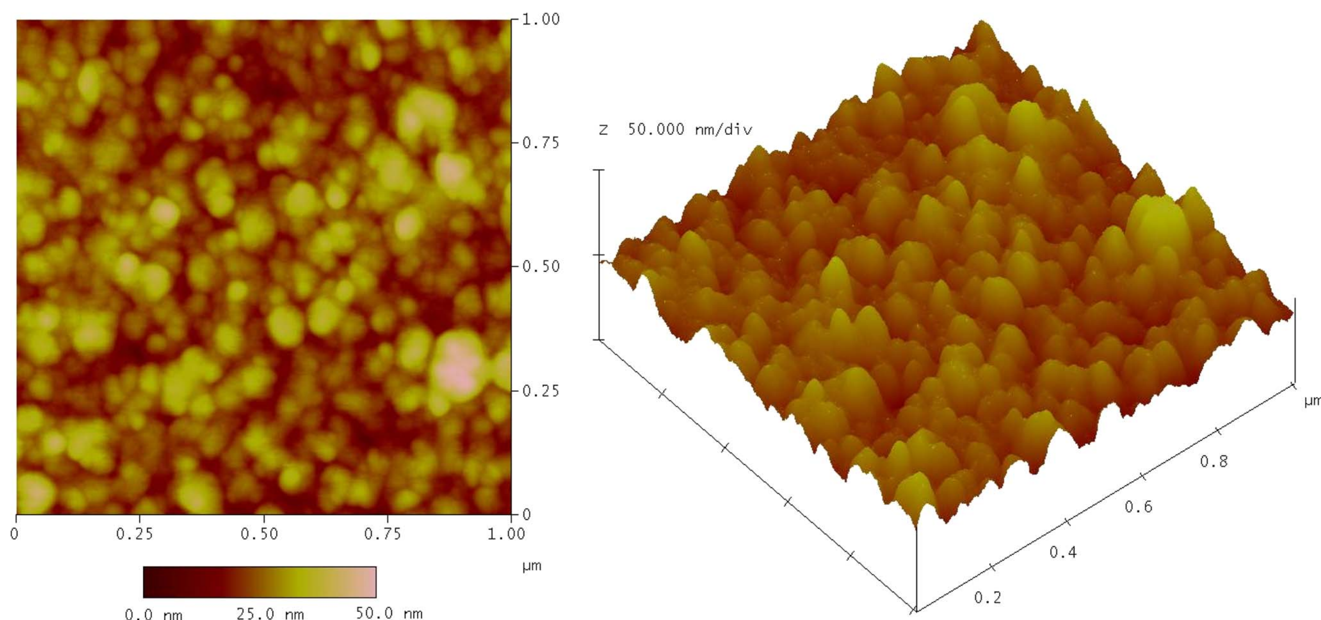

Fig. 15. Dynamic-mode imaging of a UNCD (Aqua 25) sample with the same three-faceted pyramid probe as that in Fig. 13.

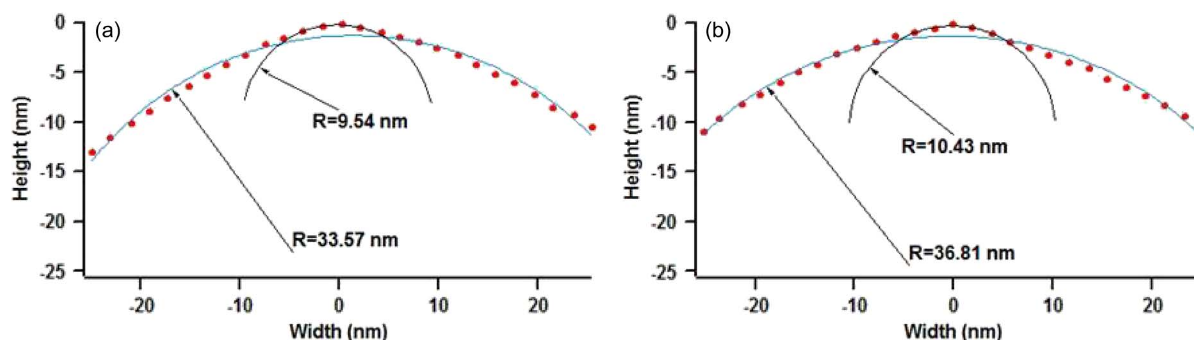

Fig. 16. SPIP tip reconstruction in two orthogonal directions from an image of the UNCD sample: (a) Transverse to the cantilever and (b) along the length of the cantilever. The fitted circles to all the 27 points shown do not capture the small protrusion at the tip and give larger values for the tip radius. Fitting a circle to the five central points captures more accurately the radius of the tip apex.

reconstructed tip profiles in the two orthogonal directions. Since both profiles are sharp close to the tip apex, fitting circles is not the best way to characterize the tip sharpness, being scale dependent. However, to provide some upper boundary numbers for tip radii, fitting circles was done over two size ranges: first, considering the whole 27 points of the SPIP reconstruction and, second, with only 5 points near the apex. Again, the radius in the transversal direction is found to be smaller than the radius in the longitudinal direction, independent of the choice for the fitting range, with a radius at the immediate apex of ∼10 nm.

A tip radius occurrence probability plot for the novel UNCD probes molded in unsharpened Si (311) V-grooves was performed based on blind tip reconstruction (SPIP) from UNCD scans, with 27 points considered for the radius fittings (clearly, an upper boundary for the radii was obtained). The results are shown in Fig. 2 (triangle markers), overlapped with the wedge size statistics for Si (100) V-grooves from a typical previous set of measurements (square markers) [25]. While, in the lower tip radius range, the improvement is incremental, the extent of the distribution curve in the larger tip radius range is reduced significantly. This is mostly visible in the average tip radius improvement (∼20 nm) for the novel probes when compared to the average wedge shape (∼62 nm) for the Si-(100)-molded probes. The near equality of the median tip radii with the average tip radii for the novel tips shows that the tip radius distribution (i.e., the derivative of the graphs presented) is symmetrical and close to a Gaussian distribution, which is a sign that the tip radius is now controlled by a single process figure of merit, likely the tip-filling accuracy.

V. Conclusion

In the present study, a novel method has been demonstrated for reliably manufacturing ultrasharp wedge-free nanoscale tips using mold pits obtained through anisotropic etching of Si (311) wafers. Contrary to commonly used molds etched in Si (100) wafers, these pits are delineated by three slow-etching Si (111) facets and form a three-sided pyramid with an isosceles triangle as the base. Since three planes always intersect at a point and never over a line, these molds provide a more consistent tip geometry that is tolerant to variations in mask shape, lithography imperfections, and angular misorientation of

the mask relative to the crystal directions. Oxidation sharpening of the pits produced sharp tips of silicon nitride and UNCD which possessed sub-10-nm tip radii and were free of wedges. Additionally, AFM probes made of UNCD based on unsharpened Si (311) molds were fabricated and tested, showing tip radii of < 10 nm (typically < 7 nm) in the direction parallel to the base of the isosceles-triangle tip cross section and < 35 nm (typically < 20 nm) in the perpendicular direction.

ACKNOWLEDGMENT

The use of the Cornell Nanofabrication Facility, a member of the National Nanotechnology Infrastructure Network, which is supported by the National Science Foundation under Grant ECS 03-35765, is acknowledged for the experimental work and probe fabrication. Part of the work benefited from the use of facilities of the Center for Nanoscale Materials, supported by the Office of Basic Energy Sciences, Office of Science, U.S. Department of Energy, under Contract DE-AC02-06CH11357. The use of the University of Pennsylvania Nano/Bio Interface Center instrumentation is acknowledged.

REFERENCES

[1] A. Boisen, J. P. Rasmussen, O. Hansen, and S. Bouwstra, "Indirect tip fabrication for scanning probe microscopy," *Microelectron. Eng.*, vol. 30, no. 1–4, pp. 579–582, Jan. 1996.

[2] J. Zou, X. Wang, D. Bullen, K. Ryu, C. Liu, and C. A. Mirkin, "A mould-and-transfer technology for fabricating scanning probe microscopy probes," *J. Micromech. Microeng.*, vol. 14, no. 2, pp. 204–211, Feb. 2004.

[3] K.-H. Kim, N. Moldovan, C. Ke, H. D. Espinosa, X. Xiao, J. A. Carlisle, and O. Auciello, "Novel ultrananocrystalline diamond probes for high resolution low-wear nanolithographic techniques," *Small*, vol. 1, no. 8/9, pp. 866–874, Aug. 2005.

[4] W. P. Kang, J. L. Davidson, M. A. George, I. Milosavljevic, J. Wittig, and D. V. Kerns, "Characterization of the microstructure of diamond pyramidal microtip emitters," *Diamond Relat. Mater.*, vol. 6, no. 2–4, pp. 403–405, Mar. 1997.

[5] K. Okano, K. Hoshina, M. Iida, S. Koizumi, and T. Inuzuka, "Fabrication of a diamond field emitter array," *Appl. Phys. Lett.*, vol. 64, no. 20, pp. 2742–2744, May 1994.

[6] W. P. Kang, J. L. Davidson, M. Howell, B. Bhuva, D. L. Kinser, D. V. Kerns, Q. Li, and J. F. Xu, "Micropatterned polycrystalline diamond field emitter vacuum diode arrays," *J. Vac. Sci. Technol. B, Microelectron. Nanometer Struct.*, vol. 14, no. 3, pp. 2068–2071, May 1996.

[7] E. Kirk, S. Tsujino, T. Vogel, K. Jefimovs, J. Gobrecht, and A. Wrulich, "Fabrication of all-metal field emitter arrays with controlled apex sizes by molding," *J. Vac. Sci. Technol. B, Microelectron. Nanometer Struct.*, vol. 27, no. 4, pp. 1813–1820, Jul. 2009.

[8] Y. Hirai, Y. Kanemaki, K. Murata, and Y. Tanaka, "Novel mold fabrication for nano-imprint lithography to fabricate single-electron tunneling devices," *Jpn. J. Appl. Phys.*, vol. 38, no. 12B, pp. 7272–7275, Dec. 1999.

[9] P. J. Holmes, *The Electrochemistry of Semiconductors*. London, U.K.: Academic, 1962.

[10] R. M. Finne and D. L. Klein, "A water–amine–complexing agent system for etching silicon," *J. Electrochem. Soc.*, vol. 114, no. 9, pp. 965–970, Sep. 1967.

[11] J. Liu, D. S. Grierson, N. Moldovan, J. Notbohm, S. Li, P. Jaroenapibal, S. D. O'Connor, A. V. Sumant, N. Neelakantan, J. A. Carlisle, K. T. Turner, and R. W. Carpick, "Prevention of nanoscale wear in atomic force microscopy through the use of monolithic ultrananocrystalline diamond probes," *Small*, vol. 6, no. 10, pp. 1140–1149, May 2010.

[12] M. Tortonese, "Cantilevers and tips for atomic force microscopy," *IEEE Eng. Med. Biol.*, vol. 16, no. 2, pp. 28–33, Mar./Apr. 1997.

[13] D.-B. Kao, J. P. McVittie, W. D. Nix, and K. C. Saraswat, "Two-dimensional thermal oxidation of silicon, II. Modeling stress effects in wet oxides," *IEEE Trans. Electron Devices*, vol. 35, no. 1, pp. 25–37, Jan. 1988.

[14] Y. Wang and D. W. van der Weide, "Microfabrication and application of high-aspect-ratio silicon tips," *J. Vac. Sci. Technol. B, Microelectron. Nanometer Struct.*, vol. 23, no. 4, pp. 1582–1584, Jul. 2005.

[15] K. Matsuyama, "Cantilever for use in a scanning probe microscope and method of manufacturing the same," U.S. Patent 5 811 017, Sep. 22, 1998.

[16] M. A. Lantz, S. J. O'Shea, and M. E. Welland, "Simultaneous force and conduction measurements in atomic force microscopy," *Phys. Rev. B, Condens. Matter*, vol. 56, no. 23, pp. 15 345–15 352, Dec. 1997.

[17] K.-H. Chung and D.-E. Kim, "Wear characteristics of diamond-coated atomic force microscope probe," *Ultramicroscopy*, vol. 108, no. 1, pp. 1–10, Dec. 2007.

[18] D. Álvarez, M. Fouchier, J. Kretz, J. Hartwich, S. Schoemann, and W. Vandervorst, "Fabrication and characterization of full diamond tips for scanning spreading-resistance microscopy," *Microelectron. Eng.*, vol. 73/74, pp. 910–915, Jun. 2004.

[19] M. Rief, H. Clansen-Schaumann, and H. E. Gaub, "Sequence dependent mechanics of single DNA molecules," *Nat. Struct. Biol.*, vol. 6, no. 4, p. 346, Apr. 1999. Biolever probes, Olympus. [Online]. Available: http://www.asylumresearch.com/Applications/LowNoise/LowNoise.pdf

[20] Olympus Probes Catalogue, Olympus Group Companies, Tokyo, Japan, p. 5, Aug. 2010.

[21] H. Shin and P. Hesketh, "Batch fabricated bifunctional AFM cantilevers for the application of SECM-AFM," presented at the 208th Meeting Electrochemical Society, Los Angeles, CA, 2005, Paper MA2005-02/AA2.

[22] P. T. Lillehei, M. A. Poggi, B. J. Polk, J. A. Smith, and L. A. Bottomley, "Plastic tip arrays for force spectroscopy," *Anal. Chem.*, vol. 76, no. 13, pp. 3861–3863, Jul. 2004.

[23] A. R. Krauss, O. Auciello, D. M. Gruen, A. Jayatissa, A. Sumant, J. Tucek, D. C. Mancini, N. Moldovan, A. Erdemir, D. Ersoy, M. N. Gardos, H. G. Busmannf, E. M. Meyer, and M. Q. Ding, "Ultrananocrystalline diamond thin films for MEMS and moving mechanical assembly device," *Diamond Relat. Mater.*, vol. 10, no. 11, pp. 1952–1961, Nov. 2001.

[24] H. Seidel, L. Csepregi, A. Heuberger, and H. Baumgartel, "Anisotropic etching of crystalline silicon in alkaline solutions, I. Orientation dependence and behavior of passivation layers," *J. Electrochem. Soc.*, vol. 137, no. 11, pp. 3612–3626, 1990.

[25] N. Moldovan, R. Divan, H. Zeng, and J. A. Carlisle, "Nanofabrication of sharp diamond tips by e-beam lithography and ICP-RIE," *J. Vac. Sci. Technol. B, Microelectron. Nanometer Struct.*, vol. 27, no. 6, pp. 3125–3131, Nov. 2009.

[26] Description of NioProbe. [Online]. Available: http://www.emsdiasum.com/microscopy/products/calibration/spm.aspx

[27] Description of TipCheck. [Online]. Available: http://www.emsdiasum.com/microscopy/products/calibration/spm.aspx

[28] Description of Aqua 25. [Online]. Available: http://www.thindiamond.com/products/uncd-wafers/uncd-aqua/

[29] Description of SPIP—Scanning Probe Image Processor. [Online]. Available: www.imagemet.com

Nicolaie Moldovan received the M.Sc. and Ph.D. degrees in physics from the University of Bucharest, Bucharest, Romania.

He completed several research stages in the Fraunhofer Institute for Solid State Technology, Munich, Germany, the Institut für Mikrotechnik Mainz, Mainz, Germany, and the Laboratoire d'Analyse et d'Architecture des Systèmes, Centre National de la Recherche Scientifique, Toulouse, France. He held the positions of Senior Researcher and Head of the Laboratory for Unconventional Microfabrication Technologies, Institute for Microtechnology, Bucharest, for several years, where he ran projects in silicon and glass micromachining, atomic-scale simulation of etching, micro-optics, and LIGA. In 1998, he joined Argonne National Laboratory, where he developed ultradeep (1 cm) LIGA technology, tilted/dynamic X-ray exposure techniques, micromachining techniques for new materials, such as ultrananocrystalline diamond (UNCD), and applications such as X-ray micro-optics, microfluidics, field emitters, and various microelectromechanical systems (MEMS). Since 2006, he has been a MEMS Lead Scientist with Advanced Diamond Technologies, Inc., Romeoville, IL, where he focuses on diamond atomic force microscopy probes and applications of UNCD. He has authored or coauthored more than 130 scientific papers.

Dr. Moldovan was the recipient of two R&D 100 Awards.

Zhenting Dai received the B.S. degree in physics from Jilin University, Changchun, China, in 1996, and the M.S. and Ph.D. degrees in physics from the Georgia Institute of Technology, Atlanta, in 2001 and 2006, respectively. For his graduate work, he microfabricated niobium mechanically controllable break junctions and successfully obtained niobium single-atom contacts.

From 2007 to 2010, he was a Postdoctoral Fellow with the Nanoengineering Laboratory, University of Illinois, Urbana. He is currently a MEMS Process Engineer with Advanced Diamond Technologies, Inc., Romeoville, IL. He is interested in ultrananocrystalline diamond (UNCD) atomic force microscopy probes and UNCD MEMS devices fabrication.

Hongjun Zeng (M'05–SM'06) received the B.S. and M.S. degrees in optics from Sichuan University, Chengdu, China, in 1994 and 1997, respectively, and the Ph.D. degree in optical engineering from the Institute of Optics and Electronics, Chinese Academy of Sciences, Chengdu, in 2000.

He is currently a Product Development Lead Scientist with Advanced Diamond Technologies, Inc., Romeoville, IL. He is the author/coauthor of more than 60 research papers and patents/disclosures. His research interests include advanced chemical vapor deposition synthesis of diamond films and their applications, micro- and nanofabrication, devices, and materials.

John A. Carlisle received the B.S. degree in physics and mathematics from Texas A&M University, Commerce, in 1986, and the Ph.D. degree in physics from the University of Illinois, Urbana, in 1993.

From 1993 to 1996, he was a Postdoctoral Research Associate with the Lawrence Livermore National Laboratory. From 2000 to 2006, he was a Physicist with Argonne National Laboratory. Over the past ten years, his work has spanned the basic–applied–commercial continuum in the area of nanostructured carbon materials, with particular focus on the synthesis and applications of ultrananocrystalline diamond (UNCD) thin films. He is the Founder and the Chief Technology Officer of Advanced Diamond Technologies, Inc. (ADT), Romeoville, IL. He has authored over 120 publications in peer-reviewed journals.

Dr. Carlisle was the recipient of four R&D 100 Awards for UNCD-based products, and ADT was named a technology pioneer in 2007 by the World Economic Forum.

Tevis D. B. Jacobs received the B.Sc. degree, with majors in mechanical engineering and materials science and engineering, from the University of Pennsylvania, Philadelphia, in 2003, the M.Phil. degree in computer modeling of materials from Churchill College, University of Cambridge, Cambridge, U.K., in 2004, and the M.Sc. degree in materials science from Stanford University, Stanford, CA, in 2006. He is currently working toward the Ph.D. degree in materials science at the University of Pennsylvania.

He worked for two years as an Engineer at Animas Corporation, a Johnson & Johnson company. His interest lies in the fundamental physics of sliding-induced wear, particularly in silicon- and carbon-based materials. Specifically, he is using atomic force microscopy and *in situ* transmission electron microscopy to carry out experiments and using principles from chemical reaction kinetics to analyze results.

Vahid Vahdat received the B.S. degree in mechanical engineering from Sharif University of Technology, Tehran, Iran, in 1998, and the M.S.E. degree from Villanova University, Villanova, PA, in 2004. He is currently working toward the Ph.D. degree in mechanical engineering at the University of Pennsylvania, Philadelphia.

From 2004 to 2008, he was a Research Specialist with the Department of Radiology, University of Pennsylvania. His research interests include nonlinear dynamics and nanoscale wear in amplitude-modulation atomic force microscopy (AFM) probes and AFM/transmission electron microscopy characterization of the probes made out of ultrananocrystalline diamond.

David S. Grierson received the B.S. degree in mathematics from the University of Wisconsin, Whitewater, in 2002, and the M.S. and Ph.D. degrees in engineering mechanics from the University of Wisconsin, Madison, in 2008.

From 2008 to 2011, he was a Postdoctoral Researcher with the Department of Mechanical Engineering, University of Wisconsin, Madison, investigating the reliability, mechanics, and scale-up of nanomembrane-based fabrication processes and scanning-probe-based nanomanufacturing. In 2010, he cofounded systeMECH, LLC, Madison, WI, a small business which focuses on developing innovative and scalable nanomanufacturing equipment and processes.

Jingjing Liu received the B.S. degree in materials science and engineering from Southwest Jiaotong University, Chengdu, China, in 2002, the M.S. degree in applied physics from the University of New Orleans, New Orleans, LA, in 2006, and the Ph.D. degree in materials science from the University of Wisconsin, Madison, in 2011.

She is currently a Process Engineer with Applied Materials, Inc., Santa Clara, CA. Her previous work has focused on atomic force microscopy/transmission electron microscopy characterization and finite-element modeling of nanoscale wear of carbon-based atomic force microscope tips.

Kevin T. Turner received the B.S. degree in mechanical engineering from The Johns Hopkins University, Baltimore, MD, in 1999, and the S.M. and Ph.D. degrees in mechanical engineering from the Massachusetts Institute of Technology, Cambridge, in 2001 and 2004, respectively.

He is an Associate Professor of mechanical engineering and applied mechanics at the University of Pennsylvania, Philadelphia. Prior to joining the University of Pennsylvania in August 2011, he was on the faculty of the Department of Mechanical Engineering, University of Wisconsin, Madison, for six years. His primary research interests are related to manufacturing and mechanic issues in micro- and nanoscale systems. His research spans multiple topics including wafer bonding, tip-based nanomanufacturing, microfluidics, and transfer and integration of semiconductor nanomembranes. He is the author of more than 30 peer-reviewed journal publications and more than 60 conference proceedings papers.

Robert W. Carpick received the B.Sc. degree in physics from the University of Toronto, Toronto, ON, Canada, in 1991, and the Ph.D. degree in physics from the University of California, Berkeley, in 1997.

He is the Chair of the Department of Mechanical Engineering and Applied Mechanics, University of Pennsylvania, Philadelphia, where he serves as a Full Professor. He moved to the University of Pennsylvania in January 2007 after serving on the faculty for seven years at the University of Wisconsin, Madison. He spent two years as a Postdoctoral Appointee at Sandia National Laboratories. He works at the intersection of mechanics, materials, and physics to study nanotribology, nanomechanics, nanostructured materials, and scanning probe microscopy. He is the author of over 80 peer-reviewed journal publications.